3D Co-N-doped hollow carbon spheres as excellent bifunctional electrocatalysts for oxygen reduction reaction and oxygen evolution reaction

Shichang Cai [a], Zihan Meng [a], Haolin Tang [a,*], Yi Wang [b,*], Panagiotis Tsiakaras [c,d,*]

[a] State Key Laboratory of Advanced Technology for Materials Synthesis and Processing, Wuhan University of Technology, Wuhan 430070, PR China
[b] The Key Lab of Low-Carbon Chemistry & Energy Conservation of Guangdong Province, School of Chemical Engineering and Technology, Sun Yat-sen University, Zhuhai 519082, PR China
[c] Laboratory of Electrochemical Devices Based on Solid Oxide Proton Electrolytes, Institute of High Temperature Electrochemistry, Yekaterinburg 620990, Russia
[d] Laboratory of Alternative Energy Conversion Systems, Department of Mechanical Engineering, School of Engineering, University of Thessaly, Pedion Areos,38834 Volos, Greece

ARTICLE INFO

ABSTRACT

Non-precious materials have been considered as promising bifunctional catalysts towards oxygen reduction reaction (ORR) and oxygen evolution reaction (OER). In the present work, a three dimensional (3D) Co-N co-doped hollow carbon sphere (HCS) electrocatalyst is synthesized at room temperature by the aid of a facile preparation method.

The as obtained Co-N co-doped catalyst exhibits excellent catalytic activity towards both ORR and OER due to its high surface area and to 3D hollow architecture. For the ORR, the catalyst shows more positive onset-potential (of ∼0.962 V *vs.* RHE) and larger diffusion limiting current density (5.55 mA cm^{-2}) compared with benchmark Pt/C catalyst in alkaline medium. Moreover, the as synthesized catalyst exhibits low potential (1.720 V *vs.* RHE) at the current density of 10 mA cm^{-2} and small Tafel slope (81 mV dec^{-1}) for OER. In addition, the catalyst exhibits remarkable methanol tolerance and good long-term stability under working conditions. This strategy provides a facile and effective method for the preparation of non-noble metal catalysts with 3D hollow structure for energy conversion and storage applications.

© 2017 Elsevier B.V. All rights reserved.

1. Introduction

In recent years, there was a growing demand for green and renewable energy [1]. Metal-air batteries, electrocatalytic water splitting, and fuel cells represent great potential applications in the field of energy conversion and storage [2,3]. However, oxygen evolution reaction (OER), occurring in the technological devices, generally exhibits sluggish reaction kinetics. As well-known, RuO_2 and IrO_2 are among the most effective OER electrocatalysts. Nevertheless, the limited availability in the earth's crust and prohibitive cost greatly hampers their large-scale applications in energy industries.

Similar to OER, oxygen reduction reaction (ORR) at the cathode of fuel cells or metal-air batteries is kinetically sluggish, which

decreases energy conversion efficiency of such devices [4–6]. The state-of-the-art catalysts for the enhancement of the ORR performance are mostly platinum based materials. Unfortunately, platinum is reserve limited and expensive. It is noteworthy that although platinum based catalysts are highly active for ORR, they show poor OER catalytic ability, while RuO_2 and IrO_2 exhibit excellent performance; however, their ORR activity is low [7]. In order to enhance the electrochemical performance of energy conversion devices, especially fuel cells and metal-air batteries, the development of low-cost non-noble metal bifunctional electrocatalysts with high electrocatalytic performance for both OER and ORR is essential [8–10].

Such kind of bifunctional catalysts are intriguing and efficient because they can decrease the cost of devices by exploiting the same kind of materials to catalyze different reactions [11]. Considerable investigations have been carried out on noble metal-free bifunctional electrocatalysts, which exhibit excellent ORR and OER electrocatalytic activity [12–15]. Three-dimensional (3D) mesoporous or macroporous nanostructures possess big surface area,

high density of exposed active sites, and abundant channels for mass transfer of reactants and products, thus being favourable for the electrocatalytic oxygen process [16–19]. Poly(methyl methacrylate) (PMMA) microsphere is one potential template to prepare 3D mesoporous architecture. Beyond that, there are several reports devoted to the synthesis of heteroatom-doped carbon as excellent ORR electrocatalysts, because of their good durability and high onset-potential compared with benchmark catalysts [20–24]. Nitrogen, oxygen, boron, sulphur, and phosphorus are non-metallic dopants and usually introduced to improve the electrocatalytic activity of carbon materials [25–28]. Among these non-metallic dopants, nitrogen is an efficient dopant that can provide numbers of structural defects and adjust the charge distribution of carbon [28,29]. Dopamine is a biocompatible molecule and contains high content of nitrogen and carbon. In alkaline media it can polymerize and adhere to almost all types of surfaces [30]. Hence, dopamine is frequently applied as the precursor for the formation of N-doped carbon materials.

However, the metal-free carbon nanomaterials usually possess relatively limited electrocatalytic ability toward OER and ORR [31,32]. To surmount this problem, non-precious metal coupled carbon-based materials have been widely studied and ordered catalysts exhibit better performance because of the improved mass transfer rate [33–35]. Up to date, Co-based composites have been recognized as OER or ORR electrocatalysts with high catalytic efficiency [36–39]. Lou et al. [40] reported the preparation of Co-N doped carbon nanotubes derived from metal-organic frameworks. The synthesized catalyst exhibited high electrocatalytic activity and stability for both ORR and OER. However, most of the Co-based catalysts showed limited electrocatalytic activities compared with noble metal-based catalysts.

In the present work, we report a facile approach to synthesize cobalt and nitrogen co-doped 3D hollow carbon spheres (HCS) using dopamine and PMMA template and a vacuum-assisted impregnation method (VIM). Polydopamine was adhered onto the surface of PMMA spheres and Co-ions subsequently were anchored on polydopamine shell [40]. After a facile carbonization process, under the protection of inert atmosphere, the catalyst was obtained. The as prepared catalyst exhibited excellent performance for both ORR and OER.

2. Experimental section

2.1. Materials

Dopamine Hydrochloride (98% pure) was purchased from Aladdin Industrial Corporation, Co(AC)$_2$ and Nafion® solution (5 wt%) were obtained from Sigma-Aldrich. The commercial 20 wt% Pt/C catalyst was obtained from Johnson Matthey Corporation. All these reagents were used as received without any further treatment.

2.2. Synthesis of NC

Briefly, dopamine (0.1 g) was stirred in a tris-buffer (20.0 mL, pH 8.5) for 0.5 h under the protection of N$_2$ flow. Then, the mixture was exposed to air for direct self-polymerization and the collected composite was labelled as PDOPA. Finally, the resulting product was carbonized at 800 °C for 5 h under N$_2$ atmosphere. The obtained sample was denoted as NC (nitrogen doped carbon).

2.3. Synthesis of N@HCS

The PMMA template was synthesized using a modified emulsifier-free emulsion polymerization method [41]. N@HCS was prepared by a vacuum-assisted impregnation method. Typically,

dopamine (0.1 g) was first stirred in a tris-buffer (20.0 mL, pH 8.5) for 0.5 h under the protection of N$_2$ flow. PMMA nanospheres were impregnated for 3 h under vacuum in the dopamine solution. The mixture was exposed to air for the self-polymerization of dopamine and the collected composite was labelled as PMMA@PDOPA. The resulting materials were finally carbonized at 800 °C for 5 h under N$_2$ atmosphere. The obtained catalyst was denoted as N@HCS.
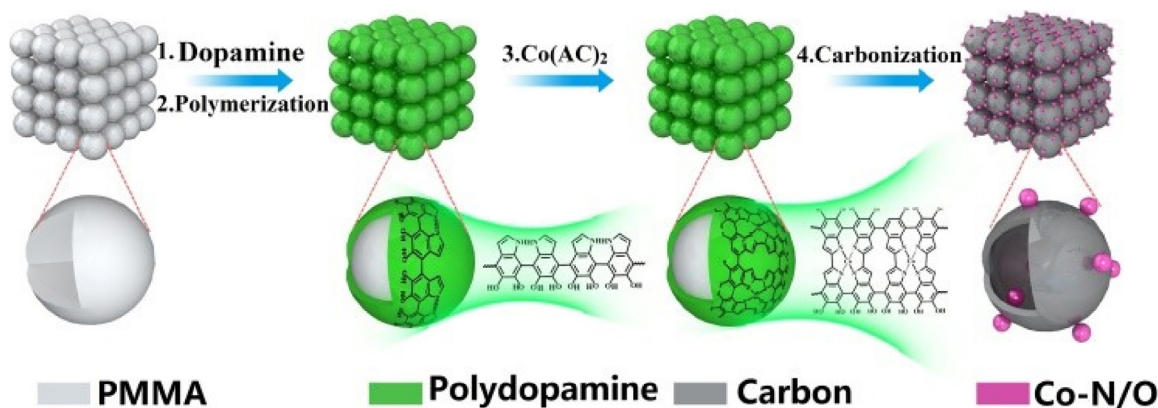
2.4. Synthesis of Co-N@HCS

Dopamine (0.1 g) was first stirred in a tris-buffer (20.0 mL, pH 8.5) for 0.5 h under the protection of N$_2$ flow. PMMA nanospheres were impregnated for 3 h under vacuum in the dopamine solution. The mixture was exposed to air for the self-polymerization of dopamine and immersed in 15.0 mL of 0.11 mol L^{-1} cobalt acetate solution by a vacuum-assisted impregnation method for another 3 h for Co introduction. The as obtained catalyst sample was denoted as Co-N@HCS.

2.5. Characterizations

In order to investigate the morphology of materials, scanning electron microscope (SEM) micrographs were taken by the aid of a Zeiss Ultra Plus instrument. Transmission electron microscopy (TEM), high resolution transmission electron microscopy (HRTEM), and element mapping images were obtained from a JEM2010-HR microscopy (FEI Tecnai G2F30). X-ray diffraction (XRD) analysis was carried out on an XRD instrument (D/MAX-RB RU-200B, Japan) using a Cu Kα (λ = 0.15406 nm) radiation source. Raman spectra were recorded using a Raman spectrometer (Gloucestershire, UK) with a 633 nm laser source. The pore properties of the samples were characterized using nitrogen adsorption-desorption isotherms performed on an ASAP 2020 instrument at 77 K. X-ray photoelectron spectroscopy (XPS) analysis was conducted on a VG Multilab 2000X-spectrometer using an Al Kα X-ray source (1486 eV).

2.6. Electrochemical measurements

Electrochemical measurements were performed by the aid of an electrochemical workstation (CHI604D, CHI instrument) with a three-electrode setup. Mercury/Mercury Oxide electrode (Hg/HgO) was used as the reference electrode, which electrode potential was 0.877 V versus reversible hydrogen electrode (RHE). A Pt plate was used as the counter electrode and a rotating disk electrode (RDE) coated with catalyst thin film as the working electrode. The catalyst ink was prepared by dispersing 3.0 mg of catalyst mixed in a solution containing 0.80 mL isopropanol, 0.20 mL deionized water and 20.0 μL Nafion® solution (5 wt%, Dupont Company). The catalyst loading was 0.3 mg cm^{-2} for both as-prepared catalysts and 20 wt% commercial Pt/C. The electrolyte was 0.1 mol L^{-1} KOH for ORR/OER tests in alkaline solution. Linear sweeping voltammetry (LSV) tests were conducted on a rotating-disk electrode (RRDE) system, in which the rotation speed varied from 400 to 2000 rpm with a scan rate of 5 mV s^{-1}. Prior to measurements, the electrolyte solution was bubbled with N$_2$ or O$_2$ at least for 30 min. The ORR stability test was carried out at 0.6 V in O$_2$-saturated electrolyte. The OER stability test was carried out at 1.6 V in O$_2$-saturated 0.1 mol L^{-1} KOH solution with a rotating speed of 1600 rpm. It should be noted that all the potentials are referred to RHE in 0.1 mol L^{-1} KOH aqueous solution without specification. The potential has been converted to the RHE scale from Hg/HgO reference electrode by the following equation: E(RHE) = E(Hg/HgO) + 0.877 V.

Scheme 1. Schematic representation for the preparation process of Co-N@HCS catalyst.

3. Results and discussion

The synthesis route of the catalyst involves mainly four steps as shown in Scheme 1. First, poly methyl methacrylate (PMMA) nanospheres are synthesized as the self-engaged template. Second, a uniform shell of polydopamine can be coated on PMMA nanospheres.

Since polydopamine has a large number of −OH and nitrogen containing functional groups [40], transition metal cations could be linked to such kind of functional groups through covalent bonds or electrostatic attraction, which is similar to the synthesis mechanism of metal-organic frameworks (MOFs) [42–44]. In the third step, Co-ions are anchored on the polydopamine shell. Finally, PMMA is removed by high temperature treatment and 3D Co-N doped hollow carbon spheres are eventually obtained. The resulting catalyst is hereafter denoted as Co-N@HCS. For comparison, the sample synthesized without PMMA template is labelled as NC and the sample synthesized without Co-ion is labelled as N@HCS. As known, there are numerous studies for the synthesis of hollow architecture using SiO_2 as hard template [20,23,45,46]. However, harsh preparation conditions, such as hydrofluoric acid or strong alkali treatment, are generally required to remove silica template. The microstructure of materials will inevitably be destroyed after the removal of SiO_2 and the acid or alkali residues may increase the risk of impairing the electrocatalytic performance of materials. Compared with the previous reports, the adopted approach here is free of harsh treatment to remove template. PMMA template is easily removed after calcination at high temperature. More importantly, the resultant 3D porous electrode exhibits excellent electrocatalytic ability for ORR/OER due to its high concentration of active sites and abundant pores for mass transfer of reactants and products.

To obtain the structural information of the as-prepared materials, SEM images of N@HCS and Co-N@HCS catalysts are shown in Fig. 1. The spherical structure of PMMA template is clearly observed in Fig. 1a. As shown in Fig. 1c, the spherical structure remains for N@HCS.

Fig. 1d shows the morphological features of Co-N@HCS, manifesting the existence of nanoparticles located at the surface or inside of the carbon spheres (Fig. 3a). Compared with that of N@HCS and Co-N@HCS catalysts, ordered spherical structure does not appear for NC (Figs. 1b and S1), indicating the important role of PMMA played in the formation of spherical structure.

The hollow spherical structure of the samples was further confirmed by the aid of TEM and by taking into account of the contrast between the inner cavity and the outer layer (Fig. 2). The TEM images (Figs. 2a and S2a–S2c) show the hollow architecture of N@HCS with an average diameter of *ca.* 372 nm. High resolution

TEM images reveal that the shell thickness is *ca.* 25 nm (Fig. 2f). Elemental mapping images in Fig. 2c–e illustrate the homogenous distribution of C, N and O. Furthermore, TEM images of Co-N@HCS catalyst (Fig. 2g–h) confirm the existence of Co-species nanoparticles located in the inner or at the surface of hollow spheres. As shown in Fig. 2i, HRTEM image of the Co-species nanoparticle has clear lattice fringes with an interspacing of 0.24 nm, corresponding to the [111] plane of CoO.

The crystal structure of the as-prepared composites was investigated by XRD (shown in Fig. 3a). Co-N@HCS, N@HCS and NC show a broad XRD peak, centered at around 25° (2θ), indicating the presence of amorphous carbon [47]. It is noteworthy that the XRD patterns of Co-N@HCS sample exhibit characteristic peaks of CoO (PDF #71-1178), while N@HCS and NC possess no discernible diffraction peaks compared with Co-N@HCS.

Based on the XRD results, it could be confirmed the efficient doping of Co element and the conversion from Co-ion to CoO after the thermal treatment. The Raman spectra of the catalysts (Fig. 3b) presented two absorption bands assigned to D and G bands (D = diamond, G = graphite). The D band ($\sim$1329 cm^{-1}) suggests the existence of substantial defects or disordered sites in the composite, whereas the G band ($\sim$1590 cm^{-1}) refers to the graphitic structure [48]. The graphitization degree of the synthesized materials can be thus characterized by the ratio of the integrated intensity (I_D/I_G). The calculated I_D/I_G ratio for Co-N@HCS catalyst is about 0.97, lower than that for N@HCS (1.04) and for NC (0.98) samples, demonstrating the higher graphitization degree of Co-N@HCS. This phenomenon could be attributed to the introduction of Co atoms in the carbon framework. In addition, Co-O vibration could be detected in the Raman spectrum of Co-N@HCS, indicating the formation of metal oxide.

The Fourier transform infrared (FT-IR) spectra were employed to understand the species of functional groups in the samples (Fig. 4a). Compared with the spectra of PMMA@PDOPA and PDOPA, the appeared new vibration band at $\sim$670 cm^{-1} for PMMA@PDOPA@Co corresponds to Co-N bond. In addition, the vibration bands of O-H bond at 3250–3500 cm^{-1} are observed for all samples, which is in agreement with molecular structure of polydopamine. These results indicate that Co-ions could be adsorbed on the polydopamine shell easily and effectively through Co-N covalent bonding.

Nitrogen adsorption-desorption isotherms were measured to investigate the pore structure of the as-synthesized materials (Fig. 4b). The adsorption isotherm obtained for Co-N@HCS catalyst exhibits a behaviour of type-IV with H1 hysteresis loop. The result indicates that Co-N@HCS catalyst has a big Brunauer-Emmett-Teller (BET) surface area of 347.3 m^2 g^{-1} with pore volume of 1.2 cm^3 g^{-1}. It is widely accepted that the porous structure is
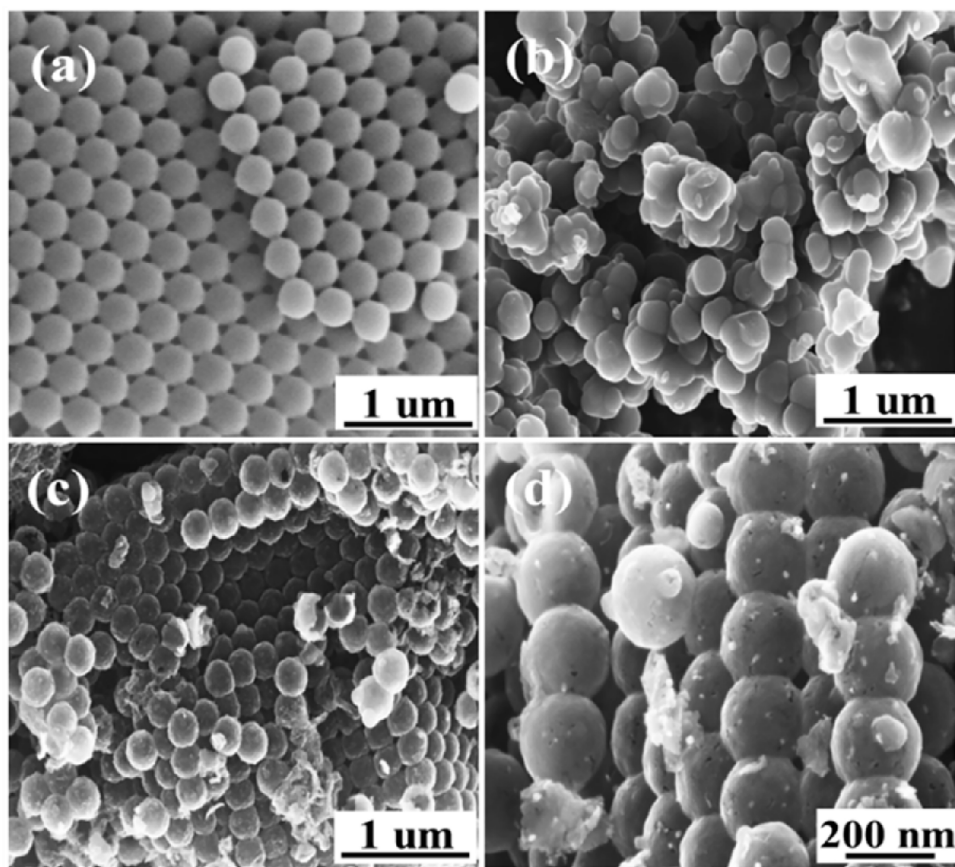
Fig. 1. SEM images of (a) PMMA, (b) NC, (c) N@HCS, and (d) as-prepared Co-N@HCS catalyst.
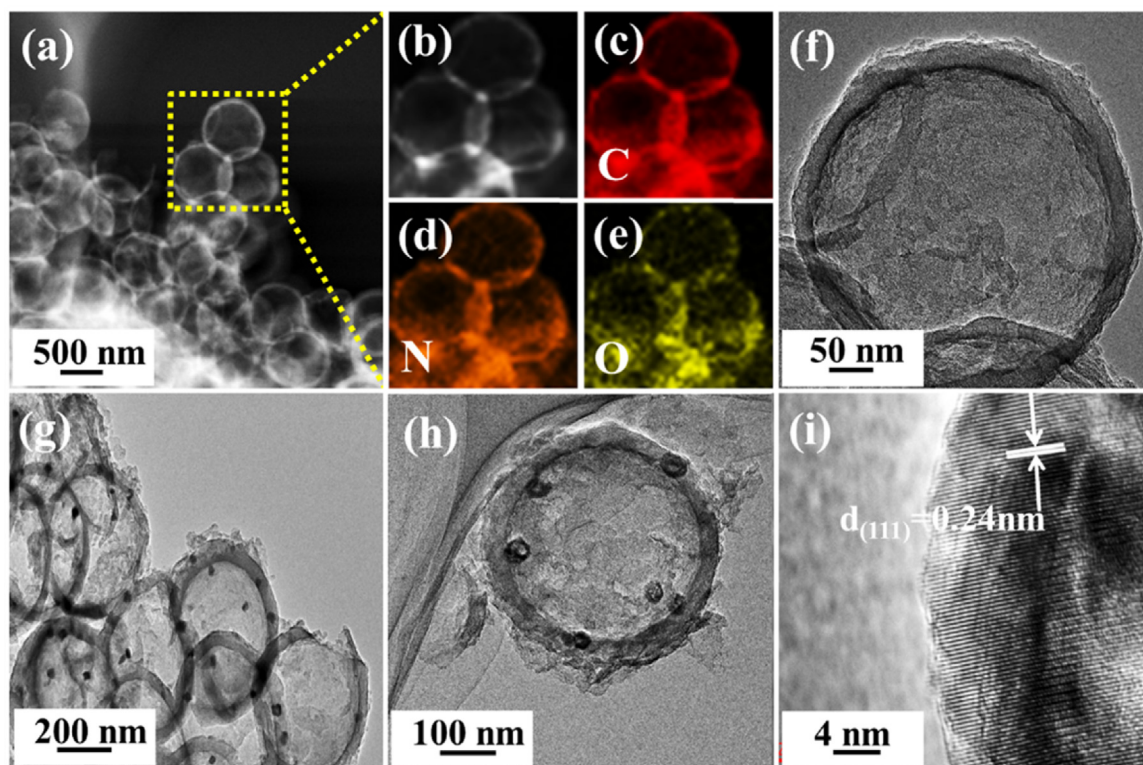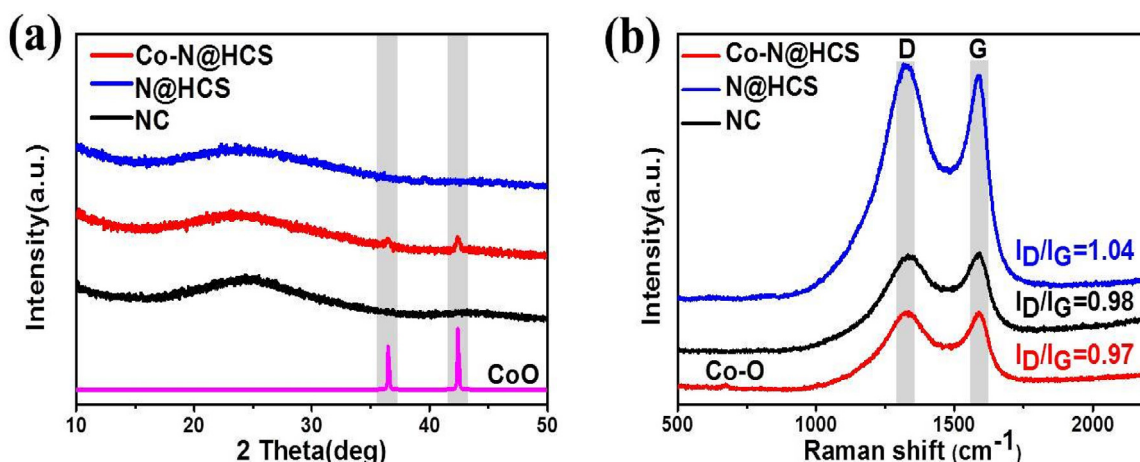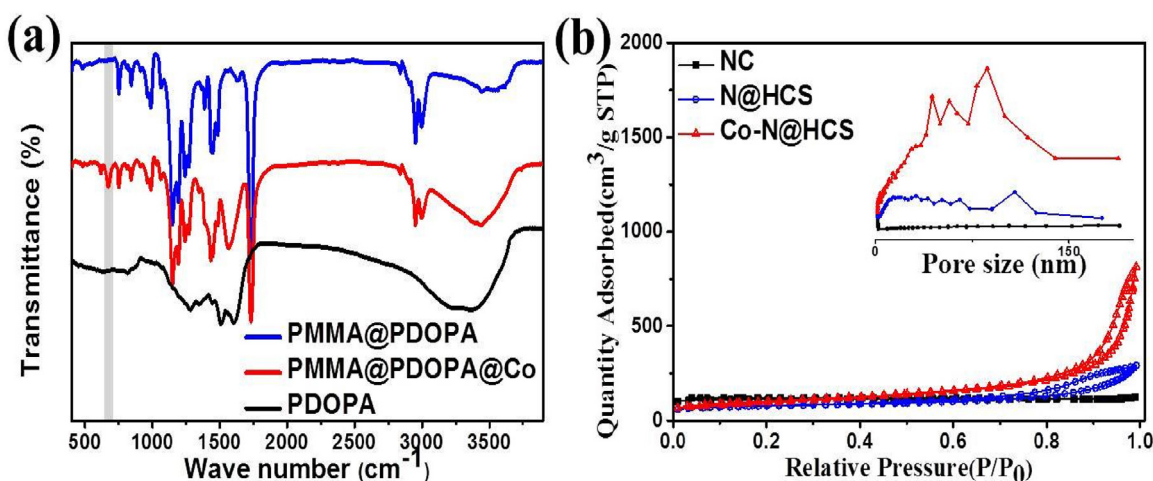
Fig. 2. TEM images (a, b and f) and elemental mapping images (c–e) of the as-prepared N@HCS sample, (g–i) TEM images of Co-N@HCS catalyst.

Fig. 3. (a) XRD patterns of Co-N@HCS, N@HCS and NC. For comparison, the standard patterns of CoO (PDF #71-1178) is also shown. (b) Raman spectra of Co-N@HCS, N@HCS and NC.

Fig. 4. (a) FT-IR spectra of PMMA@PDOPA, PMMA@PDOPA@Co and PDOPA. (b) Nitrogen adsorption-desorption isotherms of the synthesized materials. The inset is their corresponding pore size distribution.

favourable for mass transfer of reactants and products and beneficial for electrocatalytic oxygen reactions [49]. The pore size distribution curve of Co-N@HCS (inset in Fig. 4b) exhibits sharp peaks centered at about 43.8 and 86.5 nm, confirming its mesoporous and macroporous structure. For comparison, no discernible peak is observed for NC sample.

The chemical state of the elements in the composite was determined using XPS (Fig. 5). The relative element contents of Co-N@HCS and N@HCS catalysts are summarized in Table S1. The element composition of catalysts is identified from the full survey scan XPS spectra (Fig. 5a). The inset is the corresponding spectra focusing on the binding energy range from 700 to 900 eV, showing the existence of Co in more detail. High resolution C1 s spectrum (Fig. 5b) shows the presence of C-C (284.5 eV and 285.5 eV) and C-N/C-O (286.6 eV). The N1 s XPS spectrum (Fig. 5c) can be deconvoluted into four main peaks centered at 398.4, 399.9, 401.0, and 403.8 eV, assigned to pyridinic-N, pyrrolic-N, graphitic-N and pyridinic-N-oxide, respectively [50]. It is believed that carbon materials with nitrogen-doping show excellent charge mobility in the carbon atom matrix, which can accelerate the catalytic activity in electron-transfer reactions [51]. As for Co2p spectrum (Fig. 5d), the peaks at 780.8 and 786.0 eV are attributed to Co-N moieties while the peaks at 796.9 eV and 803.2 eV could confirm the presence of Co-O bond. For comparison, XPS spectra of N@HCS were

also recorded. As shown in Fig. S3, shifts in binding energy of the C1s, O1s and N1s peaks are observed for N@HCS catalyst. These differences in binding energy between N@HCS and Co-N@HCS are possibly due to the doping of Co element.

To investigate the ORR performance of the synthesized catalysts, LSV measurements were performed at different rotating speeds from 400 to 2000 rpm (Figs. S4a and S5). With the increase in rotating speed, the current density of the as-prepared catalyst increases owing to the fast diffusion rate. Koutecky-Levich (K-L) equation was applied to calculate the electron-transfer numbers of the catalyst. As depicted in Fig. S4b, the linear K-L plots reveal that Co-N@HCS catalyst shows a first-order reaction kinetics toward O_2 from 0.577 to 0.177 V. The calculated electron transfer number for ORR on Co-N@HCS catalyst is in the range of 3.78–3.98 (Fig. S4c), which is close to that of commercial Pt/C catalyst [38]. In contrast, N@HCS catalyst shows a sluggish reaction kinetics toward O_2 and the electron transfer number is in the range of 2.60–2.78 (Fig. S7c), much lower than that at Co-N@HCS catalyst. NC sample shows inferior ORR activity to N@HCS catalyst (Fig. S6a), demonstrating that the 3D porous sphere structure is favourable for the enhancement of ORR performance.

The ORR polarization curves for N@HCS, Pt/C and Co-N@HCS catalysts were recorded on RDE in O_2-saturated 0.1 mol L^{-1} KOH electrolyte (Fig. 6a). For Co-N@HCS catalyst, its ORR onset potential is about 0.962 V and limiting current density achieves
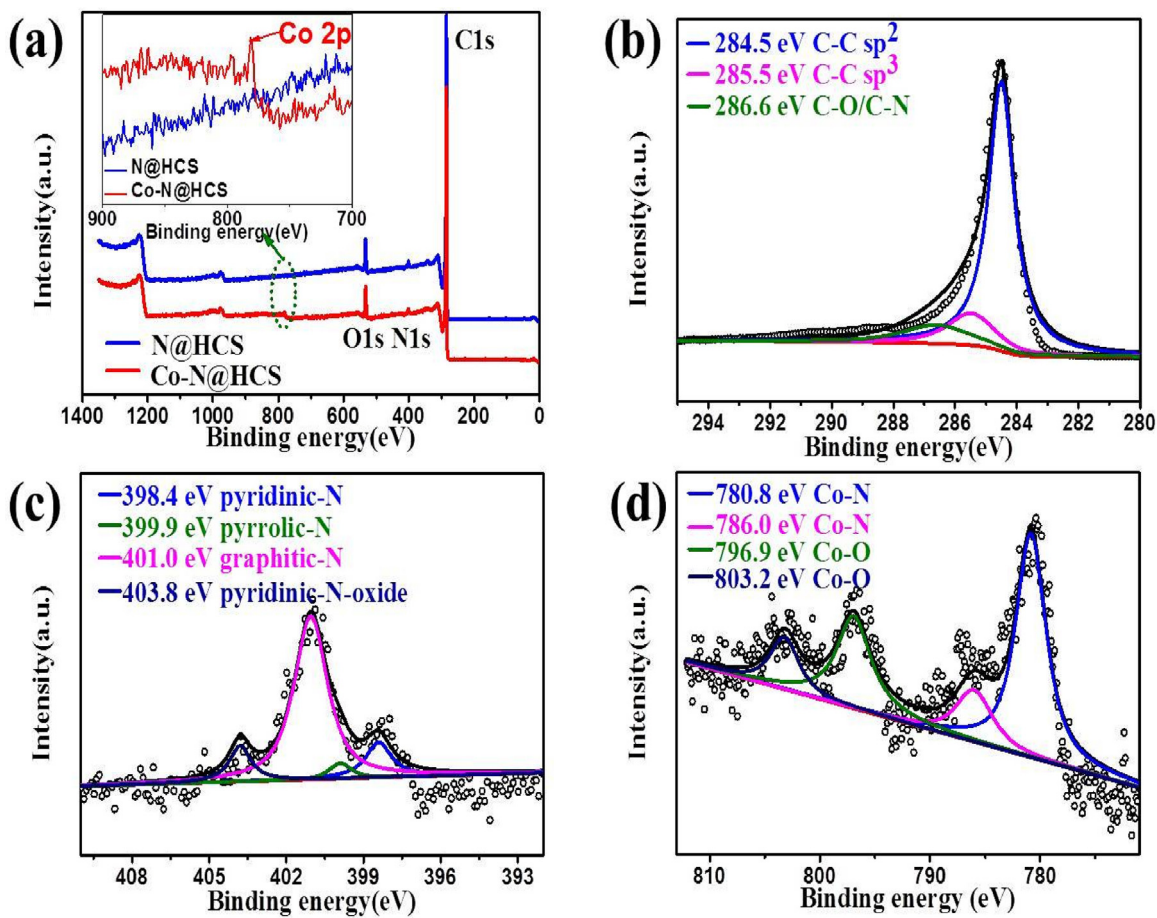
Fig. 5. XPS spectra of (a) Co-N@HCS and N@HCS catalyst and high resolution XPS spectra of (b) C1s, (c) N1s, and (d) Co2p.
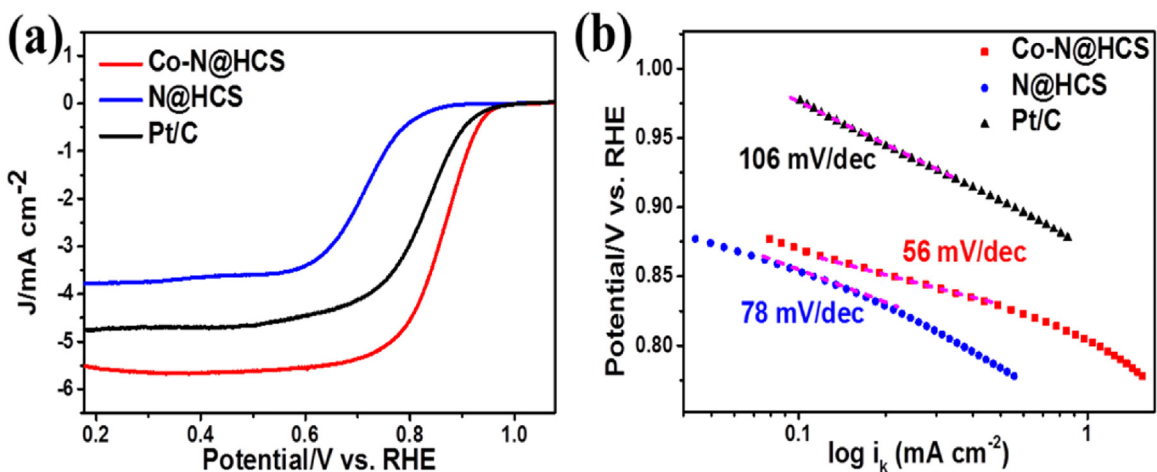

Fig. 6. (a) LSV curves of Co-N@HCS, N@HCS and commercial Pt/C catalysts in 0.1 mol L^{-1} KOH solution saturated with O$_2$ at 1600 rpm. (b) The corresponding ORR Tafel plots obtained from the ORR polarization curves.

5.55 mA cm^{-2} at a rotation speed of 1600 rpm. The positive shift of onset potential by 109 mV and the increased limiting current density by 1.62 mA cm^{-2} are observed with respect to those of N@HCS. Furthermore, the ORR performance of Co-N@HCS catalyst is also superior to that of the benchmark Pt/C catalyst (ORR onset-potential is 0.955 V and limiting current density is 4.75 mA cm^{-2}). The resulting Co-N@HCS exhibits a smaller Tafel slope (56 mV dec^{-1}) compared with that of Pt/C (106 mV dec^{-1}) and

N@HCS (78 mV dec^{-1}) (Fig. 6b), suggesting a faster rate-determined step for ORR.

The potential required for current density of 10 mA cm^{-2} (E$_{j=10}$) is generally used to evaluate OER activity. Co-N@HCS catalyst affords a current density of 10 mA cm^{-2} at a potential of ~1.720 V, which is much smaller than that of N@HCS (1.814 V) and Pt/C (1.871 V) (Fig. 7a), even comparable with the state-of-art RuO$_2$ electrocatalysts [7,52]. The inset of Fig. 7a shows the evolution of O$_2$ from the Co-N@HCS electrode at a current density of
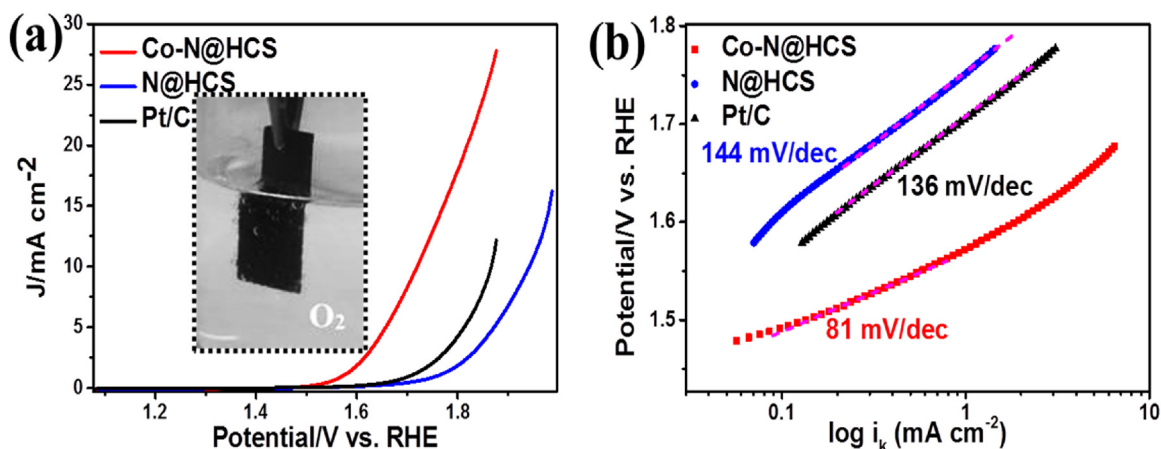
Fig. 7. A comparison of OER activities (a), and Tafel plots (b) of Co-N@HCS, N@HCS and commercial Pt/C catalyst in 0.1 mol L^{-1} KOH electrolyte at a scan rate of 5 mV s^{-1}.

10 mA cm^{-2}. Meanwhile, Tafel slope of Co-N@HCS catalyst is also smaller (81 mV dec^{-1}) than that of N@HCS (144 mV dec^{-1}) and Pt/C (136 mV dec^{-1}) catalysts (Fig. 7b), indicating the superior electrocatalytic OER kinetics of Co-N@HCS electrode.

The potential gap (ΔE) between the half-wave potential ($E_{1/2}$) for ORR and $E_{j=10}$ for OER is adopted to identify the electrocatalytic oxygen reaction performance of the as-prepared samples [53]. As can be seen in Fig. 8, Co-N@HCS shows the smallest ΔE value of 0.856 V, outperforming N@HCS (1.233 V) and commercial Pt/C catalyst (1.044 V).

These results confirm that Co-N@HCS has great potential for the reversible oxygen electrode application as an excellent and efficient bifunctional catalyst. To explore the methanol tolerance of Co-N@HCS, N@HCS, and the commercial Pt/C catalysts, the chronoamperometric method was performed at 0.6 V in 0.1 mol L^{-1} KOH electrolyte.

Fig. S7d shows the curve of commercial Pt/C that has a sharp decrease in current after the injection of methanol, indicating its poor tolerance toward methanol. While in the case of Co-N@HCS and N@HCS catalysts, the current only slightly decreases, demonstrating their outstanding tolerance toward methanol.

The ORR stability of the catalysts was performed at a potential of 0.6 V, as shown in Fig. 9a. After 10 h operation at 0.6 V, the current of the commercial Pt/C and N@HCS catalysts decreases by 23% and 57%, respectively. On the contrary, the current decrease of the as-synthesized Co-N@HCS catalyst is only 7%, indicating its great long-
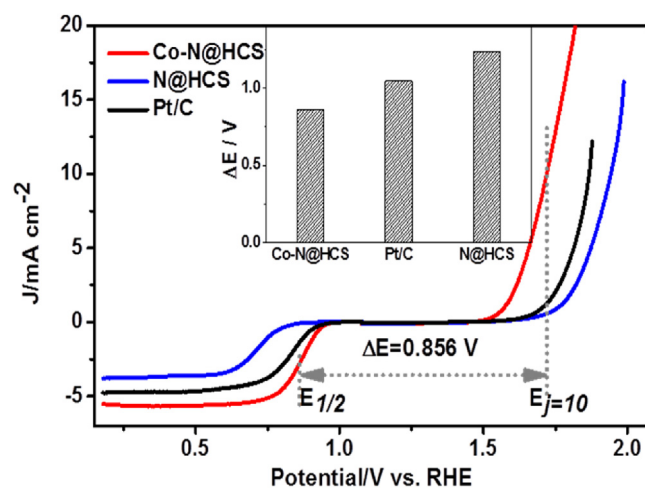

Fig. 8. The overall LSV curves of Co-N@HCS, N@HCS and commercial Pt/C catalysts in the potential range of 0.177–1.977 V, ΔE ($E_{j=10}-E_{1/2}$) isometric for bifunctional ORR and OER activities, the rotating speed is 1600 rpm. Inset: the ΔE values for Co-N@HCS, N@HCS and commercial Pt/C catalysts.

term durability. As shown in Fig. 9b, Co-N@HCS catalyst (decayed by 29%) also exhibits superior OER durability to commercial Pt/C
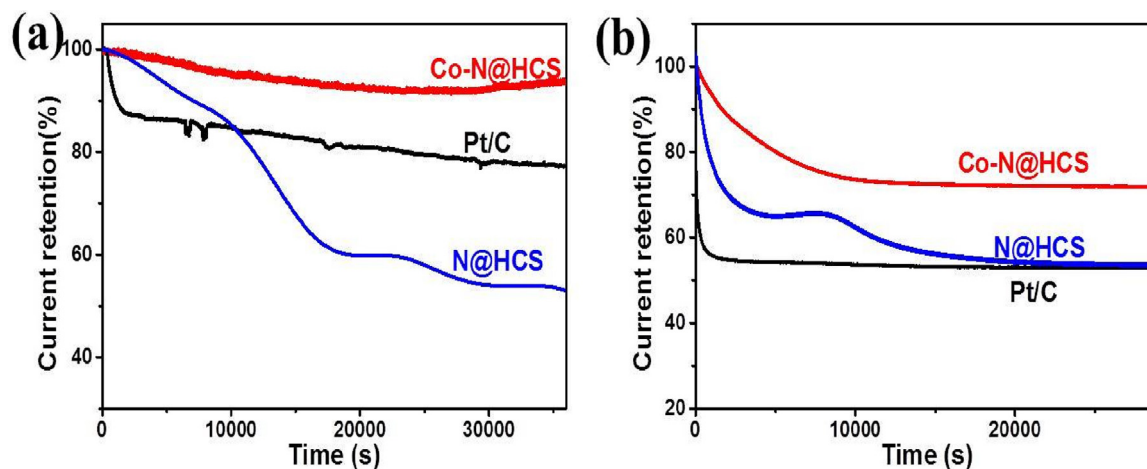

Fig. 9. (a) Current-time responses of Co-N@HCS, N@HCS and commercial Pt/C electrodes in O$_2$-saturated 0.1 mol L^{-1} KOH at 0.6 V (vs. RHE) with a rotating speed of 1600 rpm. (b) Current retention curves of Co-N@HCS, N@HCS and commercial Pt/C electrodes at 1.6 V with a rotating speed of 1600 rpm.

(decayed by 48%) and N@HCS (decayed by 46%) catalyst in 0.1 M KOH at 1.6 V after 30000 s operation.

4. Conclusions

In summary, 3D cobalt and nitrogen co-doped hollow carbon spheres were successfully synthesized in the present work by a facile preparation approach. Dopamine, acting as carbon and nitrogen source, was deposited and self-polymerized on the surface of poly(methyl methacrylate) (PMMA) nanospheres at room temperature. Transition metal cobalt was then cooperated to improve the catalytic activity of the sample. The unique hollow sphere architecture of Co-N@HCS catalyst highly and efficiently enables its activities for both ORR and OER. Moreover, Co-N@HCS catalyst exhibited excellent methanol tolerance and durability for ORR/OER in alkaline electrolyte. This work may provide a new viewpoint for the design and preparation of 3D non-precious metal based bifunctional catalysts for energy conversion and storage devices.

Acknowledgements

Appendix A. Supplementary data

Supplementary data associated with this article can be found, in the online version, at http://dx.doi.org/10.1016/j.apcatb.2017.06.008.

References

[1] Z. Chen, D. Higgins, A. Yu, L. Zhang, J. Zhang, Energy Environ. Sci. 4 (2011) 3167–3192.
[2] J. Smagorinsky, Energy Environ. Sci. 7 (2014) 3519–3542.
[3] J. Ran, J. Zhang, J. Yu, M. Jaroniec, S.Z. Qiao, Chem. Soc. Rev. 43 (2014) 7787–7812.
[4] X. Ge, A. Sumboja, D. Wuu, T. An, B. Li, F.W.T. Goh, T.S.A. Hor, Y. Zong, Z. Liu, ACS Catal. 5 (2015) 4643–4667.
[5] H.A. Gasteiger, S.S. Kocha, B. Sompalli, F.T. Wagner, Appl. Catal. B: Environ. 56 (2005) 9–35.
[6] S.H. Dong, D. He, W. Jing, L. Yue, P. Yin, H. Xun, Y. Wu, Y. Li, J. Am. Chem. Soc. 138 (2016) 2008–2010.
[7] Z. Jiang, Z.J. Jiang, T. Maiyalagan, A. Manthiram, J. Mater. Chem. A 4 (2016) 5877–5889.
[8] J. Yang, H. Sun, H. Liang, H. Ji, L. Song, C. Gao, H. Xu, Adv. Mater. 28 (2016) 4606–4613.
[9] H. Tang, Y. Zeng, D. Liu, D. Qu, J. Luo, K. Binnemans, D.E.D. Vos, J. Fransaer, D. Qu, S.G. Sun, Nano Energy 26 (2016) 131–138.
[10] Z. Zhuang, W. Sheng, Y. Yan, Adv. Mater. 26 (2014) 3950–3955.
[11] F. Meng, H. Zhong, D. Bao, J. Yan, X. Zhang, J. Am. Chem. Soc. 138 (2016) 10226–10231.
[12] Y. Gorlin, T.F. Jaramillo, J. Am. Chem. Soc. 132 (2010) 13612–13614.
[13] J. Zhang, Z. Zhao, Z. Xia, L. Dai, Nat. Nanotechnol. 10 (2015) 444–452.
[14] H. Tang, Y. Zeng, Y. Zeng, R. Wang, S. Cai, C. Liao, H. Cai, X. Lu, P. Tsiakaras, Appl. Catal. B: Environ. 202 (2011) 550–556.
[15] P. Yin, T. Yao, Y. Wu, L. Zheng, Y. Lin, W. Liu, H. Ju, J. Zhu, X. Hong, Z. Deng, Angew. Chem. Int. Ed. 55 (2016) 10800–10805.
[16] S. Lee, D.H. Kwak, S.B. Han, E.T. Hwang, M.C. Kim, J.Y. Lee, Y.W. Lee, K.W. Park, Electrochim. Acta 191 (2016) 805–812.
[17] T. Sun, L. Xu, S. Li, W. Chai, Y. Huang, Y. Yan, J. Chen, Appl. Catal. B: Environ. 193 (2016) 1–8.
[18] B.B. Li, Y.Q. Liang, X.J. Yang, Z.D. Cui, S.Z. Qiao, S.L. Zhu, Z.Y. Li, K. Yin, Nanoscale 7 (2015) 16704–16714.
[19] J. Wang, Z. Wu, L. Han, R. Lin, W. Xiao, C. Xuan, H.L. Xin, D. Wang, J. Mater. Chem. A 4 (2016) 5678–5684.
[20] G.A. Ferrero, K. Preuss, A. Marinovic, A.B. Jorge, N. Mansor, D.J. Brett, A.B. Fuertes, M. Sevilla, M.M. Titirici, ACS Nano 10 (2016) 5922–5932.
[21] Y. Su, Z. Yao, F. Zhang, H. Wang, Z. Mics, E. Cánovas, M. Bonn, X. Zhuang, X. Feng, Adv. Funct. Mater. 26 (2016) 5893–5902.
[22] M. Li, Y. Xiong, X. Liu, C. Han, Y. Zhang, X. Bo, L. Guo, J. Mater. Chem. A 3 (2015) 9658–9667.
[23] J.C. Li, S.Y. Zhao, P.X. Hou, R.P. Fang, C. Liu, J. Liang, J. Luan, X.Y. Shan, H.M. Cheng, Nanoscale 7 (2015) 19201–19206.
[24] K. Parvez, S. Yang, Y. Hernandez, A. Winter, A. Turchanin, X. Feng, K. Müllen, ACS Nano 6 (2012) 9541–9550.
[25] D. Voiry, J. Yang, M. Chhowalla, Adv. Mater. 28 (2016) 6197–6206.
[26] T.Y. Ma, J. Ran, S. Dai, M. Jaroniec, S.Z. Qiao, Angew. Chem. Int. Ed. 54 (2015) 4646–4650.
[27] J. Wu, M.T. Rodrigues, R. Vajtai, P.M. Ajayan, Adv. Mater. 28 (2016) 6239–6246.
[28] Y. Jiao, Y. Zheng, M. Jaroniec, S.Z. Qiao, J. Am. Chem. Soc. 136 (2014) 4394–4403.
[29] D. Guo, R. Shibuya, C. Akiba, S. Saji, T. Kondo, J. Nakamura, Science 351 (2016) 361–365.
[30] H. Tang, M. Xiong, D. Qu, D. Liu, Z. Zhang, Z. Xie, X. Wei, W. Tu, D. Qu, Nano Energy 15 (2015) 75–82.
[31] Y. Zheng, Y. Jiao, M. Jaroniec, Y. Jin, S.Z. Qiao, Small 8 (2012) 3550–3566.
[32] D.W. Wang, D. Su, Energy Environ. Sci. 7 (2014) 576–591.
[33] G. Zhang, Y. Song, H. Zhang, J. Xu, H. Duan, J. Liu, Adv. Funct. Mater. 26 (2016) 3012–3020.
[34] T. Jiang, Y. Wang, K. Wang, Y. Liang, D. Wu, P. Tsiakaras, S. Song, Appl. Catal. B: Environ. 189 (2016) 1–11.
[35] K. Wang, Y. Wang, Z. Liang, Y. Liang, D. Wu, S. Song, P. Tsiakaras, Appl. Catal. B: Environ. 147 (2014) 518–525.
[36] W. Zhao, P. Yuan, X. She, Y. Xia, S. Komarneni, K. Xi, Y. Che, X. Yao, D. Yang, J. Mater. Chem. A 3 (2015) 14188–14194.
[37] Z. Wang, B. Li, X. Ge, F.W. Goh, X. Zhang, G. Du, D. Wuu, Z. Liu, T.S. Andy Hor, H. Zhang, Y. Zong, Small 12 (2016) 2580–2587.
[38] H. Tang, S. Cai, S. Xie, Z. Wang, Y. Tong, M. Pan, X. Lu, Adv. Sci. 3 (2015) 1487–1498.
[39] Y. Liang, Y. Li, H. Wang, J. Zhou, J. Wang, T. Regier, H. Dai, Nat. Mater. 10 (2011) 780–786.
[40] L. Yang, J. Kong, D. Zhou, J.M. Ang, S.L. Phua, W.A. Yee, H. Liu, Y. Huang, X. Lu, Chem. –Eur. J. 20 (2014) 7776–7783.
[41] H. Li, L. Zhang, H. Dai, H. He, Inorg. Chem. 48 (2009) 4421–4434.
[42] J.K. Sun, Q. Xu, Energy Environ. Sci. 7 (2014) 2071–2100.
[43] D. Umeyama, S. Horike, M. Inukai, Y. Hijikata, S. Kitagawa, Angew. Chem. Int. Ed. 50 (2011) 11706–11709.
[44] C. Sanchez, B. Julián, P. Belleville, M. Popall, J. Mater. Chem. 15 (2005) 3559–3592.
[45] L. Shang, H. Yu, X. Huang, T. Bian, R. Shi, Y. Zhao, G.I. Waterhouse, L.Z. Wu, C.H. Tung, T. Zhang, Adv. Mater. 28 (2016) 1668–1674.
[46] X. Gao, Z. Chen, Y. Yao, M. Zhou, Y. Liu, J. Wang, W.D. Wu, X.D. Chen, Z. Wu, D. Zhao, Adv. Funct. Mater. 26 (2016) 6649–6661.
[47] F. Bai, Y. Xia, B. Chen, H. Su, Y. Zhu, Carbon 79 (2014) 213–226.
[48] Z. Huang, H. Zhang, Y. Chen, W. Wang, Y. Chen, Y. Zhong, Electrochim. Acta 108 (2013) 421–428.
[49] N.D. Kim, W. Kim, B.J. Ji, S. Oh, P. Kim, Y. Kim, J. Yi, J. Power Sources 180 (2008) 671–675.
[50] J. Wei, Y. Hu, Y. Liang, B. Kong, J. Zhang, J. Song, Q. Bao, G.P. Simon, S.P. Jiang, H. Wang, Adv. Funct. Mater. 25 (2015) 5768–5777.
[51] O.Y. Podyacheva, Z.R. Ismagilov, Catal. Today 249 (2015) 12–22.
[52] J. Zhang, Z. Zhao, Z. Xia, L. Dai, Nat. Nanotechnol. 10 (2015) 444–452.
[53] S. Chen, J. Duan, Y. Zheng, X. Chen, X.W. Du, M. Jaroniec, S.Z. Qiao, Energy Storage Mater. 1 (2015) 17–24.